Faraday
Discussions

Structural Evolution of TiN Catalysts during Mechanocatalytic Ammonia Synthesis

Journal:	*Faraday Discussions*
Manuscript ID	FD-ART-11-2022-000164.R1
Article Type:	Paper
Date Submitted by the Author:	06-Dec-2022
Complete List of Authors:	DeWitt, Jacobg; Georgia Institute of Technology, School of Chemical and Biological Engineering Phillips, Erin; Georgia Institute of Technology, School of Chemistry and Biolchemistry Hebisch, Karoline; Georgia Institute of Technology, School of Chemical and Biological Engineering Tricker, Andrew; Georgia Institute of Technology, School of Chemical and Biological Engineering Sievers, Carsten; Georgia Institute of Technology, School of Chemical and Biological Engineering

SCHOLARONE™
Manuscripts

Structural Evolution of TiN Catalysts during Mechanocatalytic Ammonia Synthesis

Jacob A. DeWitt[1], Erin V. Phillips[2], Karoline L. Hebisch[1], Andrew W. Tricker[1*], Carsten Sievers[1]*

[1]*School of Chemical & Biomolecular Engineering, Georgia Institute of Technology, Atlanta, GA 30332 (U.S.A.)*
[2]*School of Chemistry and Biochemistry, Georgia Institute of Technology, Atlanta, GA 30332 (U.S.A.)*
*carsten.sievers@chbe.gatech.edu, awtricker@gmail.com

Abstract

Mechanocatalytic ammonia synthesis is a novel approach toward ammonia synthesis under mild conditions. However, many open questions remain about the mechanism of mechanocatalytic ammonia synthesis as well as the structure of the active catalysts during milling. Herein, the structural evolution of an *in-situ* synthesized titanium nitride catalyst is explored during extended milling. The yield of ammonia bound to the catalyst surface was found to strongly correlate with an increase in catalyst surface area during milling, although a lower surface concentration of ammonia at earlier milling times suggests a delay in ammonia formation, corresponding to the conversion of the titanium metal pre-catalyst into the nitride. Small pores develop in the catalyst during milling due to interstitial spaces between agglomerated titanium nitride nanoparticles as shown by SEM and TEM. In the first 6 h, the titanium is both converted to a nitride and fractured to smaller particles, before an equilibrium state is reached. After 18 h of milling, the catalyst nanoparticles appear to crystallize to a denser material, resulting in a loss of surface area and pore volume.

Introduction

Virtually all of the world's ammonia is currently produced by the Haber-Bosch process, which accounts for approximately 1% of global CO_2 emissions.[1,2] Ammonia synthesis is burdened by two competing factors: the high energy needed to activate the very stable N_2 triple-bond and increasing thermodynamic limitations with increasing temperature.[3] While catalysts and advanced reaction engineering have allowed for an economically viable process, harsh reaction conditions (>375 °C, >100 atm) must still be used, which can only be economically viable in large-scale, centralized plants. With this constraint, local ammonia production is not currently feasible in developing regions, resulting in high costs and hazards for transportation of fertilizers and limited agricultural output in certain regions. For this reason, significant effort has been devoted to developing processes that operate under milder conditions. More active ammonia synthesis catalysts would allow for a lower reaction temperature, which would lead to a higher equilibrium conversion in thermochemical processes. Besides Ru-based catalysts,[4] much attention has been focused on transition metal nitrides.[5] Binary nitrides of Mo,[6,7] U,[8] V,[9] Rh[10] and Ce[11] also showed activity in thermal catalytic ammonia synthesis reactions. Even better performance was observed over ternary nitrides like Co_3Mo_3N [5,12,13] and Ni_2Mo_3N.[14] Nørskov *et al.* explained the high activity of CoMo-based catalysts with a nearly optimal nitrogen adsorption energy that allows these materials to activate N_2 but also to desorb NH_3 as the product.[13] Additionally, several

alternative reaction systems have been proposed, including photocatalysis[15], electrocatalysis[16], and plasma-assisted catalysis.[17] Photocatalytic approaches suffer from low yields, while electrochemical methods experience low efficiencies due to the competing hydrogen evolution reaction.[18] For plasma-assisted catalysis, moving the technology out of the laboratory remains a hurdle.[19] As of now, none of these approaches have a clear pathway to become a dominant, low-intensity ammonia synthesis technology commercially.

Mechanochemistry has shown considerable promise in supplying a sustainable manufacturing pathway for a variety of chemicals ranging from small organic molecules to commodity chemicals.[20-22] In recent years, mechanochemistry has proven to be a novel method for the synthesis of various materials and chemicals such as MOFs,[22] organic molecules,[23] pharmaceutical and agricultural compounds[24, 25], and nanomaterials[26], as well as a platform for producing renewable chemicals via plastics depolymerization[27, 28] or biomass deconstruction.[29-31] An appealing aspect of mechanochemistry is the ability to conduct reactions that usually require intense reaction conditions at nominally ambient conditions. These reactions are typically performed using ball mill reactors, where the collisions can create reaction environments that reach high local temperatures, but only persist for tens of milliseconds.[32] These short-lived reaction environments can also directly affect the activity of catalysts by creating highly reactive, transient surfaces.[33, 34] Hence, given the demonstrated advantages and recent work, mechanochemistry has been identified as a candidate for ammonia production at nominally ambient conditions. Ammonia synthesis under mild conditions could mitigate these drawbacks through smaller-scale, modular reactors by allowing for near end-use production.

Several groups have reported that milling various transition metals in a nitrogen atmosphere results in mechanochemical nitrogen activation and the formation of transition metal nitrides. Roldan *et al.* described the formation of vanadium nitride with a high purity (96%) from vanadium metal at nominally ambient temperature for milling times between 0.5 and 8 h.[35] Welham *et al.* used Ti- and FeTi-oxides to form homogeneous nanocrystalline titanium nitride-alumina composites at ambient temperatures by milling pure titanium nitride and alumina in a rotary ball mill for 100 h.[36] Jacobsen *et al.* provided a successful example for synthesis of the ternary nitrides Co_2Mo_3N and Fe_3Mo_3N starting from the secondary nitride material Mo_2N and the transition metal after milling between 0.5 and 90 h.[37] These groups showed that commonly used mechanochemical setups are capable of activating nitrogen to form metal nitrides from various transition metals. None of these groups, however, explored the potential of mechanochemical hydrogenation of these nitrides to ammonia.

The history of mechanocatalytic ammonia synthesis on the other hand is brief and relatively limited in scope. First mentions of mechanochemical synthesis can be traced to reports by Heinicke *et al.* (1961 and 1974).[38, 39] Their first paper introduced the basic concept of mechanocatalytic ammonia synthesis from the elements in stoichiometric quantities over an industrial Haber-Bosch catalyst in a "vacuum grain-beam apparatus".[38] The group showed in their second paper that initially, the addition of water had a promoting influence on ammonia formation, but eventually their iron catalyst was oxidized, leading to a decline in the promoting effect. The group reported stable ammonia formation rates after an activation period of 8 - 9 h. However, little mechanistic

insight of either the nitrogen activation or hydrogenation was provided, as the group speculated that a "triboplasma" is generated, or that the reaction is driven by electrons generated through mechanical attrition.

In the last few years, exploration of ammonia synthesis via mechanochemistry has rapidly increased, with several publications in short succession.[40-42] Tricker *et al.* reported nitrogen fixation and subsequent direct ammonia synthesis over an *in situ* formed titanium nitride catalysis via a continuous gas flow system for up to 12 h.[40] The group used a vibratory ball mill at ambient conditions, *i.e.*, neither externally heated nor pressurized. X-ray powder diffraction (XRD) and X-ray absorption spectroscopy (XAS) revealed the rapid, near quantitative conversion of metallic titanium powder to titanium nitride within 4.5 h, which acts as the catalyst. Ammonia formation was reported in the gas phase and on the catalyst surface. The process starts with an induction period because a minimum extent of nitridation is necessary to yield a measurable quantity of ammonia. After probing the thermodynamics of ammonia formation in a thermally catalyzed system, and comparing their mechanocatalytic rates with thermodynamic equilibrium calculations, the group proposed a transient Mars-van Krevelen mechanism, in contrast to the thermochemical Langmuir-Hinshelwood assumption. Here, collisions create highly energetic local environments for N_2 activation. Relaxation of the activated material brings the TiN into a different thermodynamic regime, where it can undergo hydrogenation and NH_3 is formed.[32, 40] This contribution delivered the first mechanistic understanding of mechanocatalytic ammonia formation over transition metal nitrides. While the need for converting the titanium metal pre-catalyst into a nitride phase was illustrated, the exact nature of the active phase was not identified.

Han *et al.* reported increased gas phase ammonia concentration (82.5 vol% at nominally ambient reaction conditions of 1 bar and 45 °C) due to a mechanically induced chemical looping synthesis.[41] In a two-step process, iron-powder was milled in a pure N_2 atmosphere, where nitrogen dissociated on collision-induced, low-coordinated iron defect sites as a direct result of mechanochemical activation. In a subsequent step, the vessel atmosphere was replaced with H_2, and milling induced hydrogenation of the adsorbed nitrogen to form ammonia. Analysis of the iron materials with Mössbauer spectroscopy, X-ray photoelectron spectroscopy (XPS) and X-ray absorption near edge structure (XANES) showed that the active species in this reaction are located on the iron surface in the form of adsorbed nitrogen, but the bulk material is not converted into iron nitride and does not contribute significantly toward ammonia production. The authors proposed a reaction mechanism that closely resembles a thermocatalytic route. However, similar to the mechanism proposed by Tricker *et al.*,[40] the dynamic changes in the catalyst, induced by milling, significantly lowered activation barriers during the hydrogenation reactions, as calculated by DFT.

Schüth *et al.* demonstrated continuous ammonia formation for up to 65 h over various iron-based and bimetallic alloys.[42] The highest performance (*i.e.*, a yield of 0.3% ammonia in the gas phase) was found over an iron catalyst promoted with 2.2 mol% Cs. The group speculates that the electron donating capability of the heavy alkali metal Cs was responsible for the promoting effect. Their analysis suggested a mechanism closer to the surface-activation of nitrogen that is found in the conventional Haber-Bosch process rather than the formation of bulk-nitrides. However,

pressures of between 20-170 bar were necessary to achieve the reported yields, while truly ambient conditions only led to an ammonia yield of 0.04 %.

He *et al.* recently reported the mechanochemical synthesis of ammonia by milling water with nitrogen gas in a planetary ball mill in the absence of an explicit catalyst with a rate up to of 2.8 mg L^{-1} h^{-1}.[43] They revealed that abrasion of the milling vessel and grinding balls formed an iron containing powder in the suspension, which acted as the active material. The oxidation of metal shavings with water during ball milling to facilitate hydrogenation reactions, primarily of organic compounds, has been used several times before,[44, 45] but this was the first application of this approach to nitrogen hydrogenation. Variation of milling parameters showed that the ammonia formation rate increased with rotational speed, but an optimal ball loading existed. Too few balls lead to fewer collisions, while too many balls lead to interference, resulting in inefficient kinetic energy transfer into the active material. The authors claimed that characterization of the iron powder after reaction showed the presence of activated nitrogen species on the surface and proposed a reaction pathway in which adsorbed N_2 is first hydrogenated followed by the dissociation of the N≡N bond.

The studies discussed above show that efficient nitrogen fixation and unique solid-solid interactions are key factors in the development of successful mechanochemical ammonia synthesis. However, the nature of transient active sites and structural evolution of catalysts during extended milling remains understudied. This contribution elucidates the structural evolution of TiN catalysts with increasing milling time up to 18 h.

Experimental

Ammonia Synthesis and Quantification

H_2 and N_2 gases of grade 5 (ultra-high purity, UHP) were acquired from AirGas. Titanium nitride (TiN) powder (99.7% trace metal basis) was purchased from Alfa Aesar. Titanium powder (Ti) (100 mesh, 99.7% trace metals basis) was acquired from Sigma-Aldrich. All metals were stored in a desiccator to reduce atmospheric exposure and oxidation.

All milling experiments were conducted in a Retsch MM400 vibratory ball mill with a 25 mL stainless steel reaction vessel with one grinding ball (d=20 mm). All reactions were performed at a milling frequency of 30 Hz, and a total gas flow of 15 sccm. The metal powders were milled in equimolar gas flows of N_2 and H_2. No external heating or pressurization was performed at any point in the experimental procedure.

Ammonia quantification was conducted by a Thermo Scientific Dionex Aquion Ion Chromatography (IC) System with an anionic polymer column (Dionex IonPac AS22, cation column) using Chromelon Chromatography Studio 7 processing software. An ammonia standard solution of 1.00 mg L^{-1} as NH_3-N by Hach Company was utilized for calibration. IC samples were prepared as a suspension of 1 mg mL^{-1} catalyst in deionized (DI) water. This solution was sonicated for 45 min, then centrifuged for 20 min at 13000 rpm. The liquid supernatant was removed and filtered using a 0.2 μm pore sized nylon membrane syringe filter. 5 mL of the

washing solution was then injected into the IC column using a 20 mmol methanesulfonic acid eluent (Sigma Aldrich, ≥99.0%) in DI water.

SEM/EDS

Scanning electron microscopy with Energy dispersive X-ray spectroscopy (SEM/EDS) was conducted using a Thermo Axia Variable Pressure SEM equipped with a thermionic tungsten filament source, and a coupled EDS X-ray detector. The samples were examined under a high vacuum at a voltage of 10.00 kV using an Everhart–Thornley detector (ETD) for SEM imaging and a working distance of 9.4 – 10.4 mm. EDS spectra were acquired using quantitative elemental mapping with a scan time of 60 s for each specified area.

TEM/EDS

Transmission electron microscopy with Energy dispersive X-ray spectroscopy (TEM/EDS) was performed using a FEI Tecnai F30 TEM equipped with a thermally assisted field emission (TFE) operating at 300 kV. Images were captured using a Gatan GIF system (Tridiem 863 UHS) and element mapping was performed by a thin window EDS spectrometer.

N_2 Physisorption

Nitrogen physisorption with Brunauer-Emmett-Teller (BET) analysis[46] was performed using a Micromeritics ASAP 2020 Accelerated Surface Area and Porosimetry System. Analysis was conducted for 0.100 g of material that was degassed under a vacuum of 10 mmHg for 200 min before analysis.

Results and Discussion

The yield of ammonia bound to TiN after different milling times is shown in Figure 1. Between 3 and 6 h, the yield of adsorbed ammonia increased from 0.4 to 1.2 mg NH_3 per g catalyst, after which the yield remained constant, indicating that any additional ammonia formation was balanced by removal of the product in the continuous gas stream through the milling vessel. The lower ammonia formation in the first 3 h is expected, since the Ti metal pre-catalyst had to be converted to an active TiN catalyst prior to ammonia formation. If the catalyst had become inactive after the first 6 h, a steady decrease in adsorbed ammonia yield would be expected instead, due to continuous desorption into the gas phase.
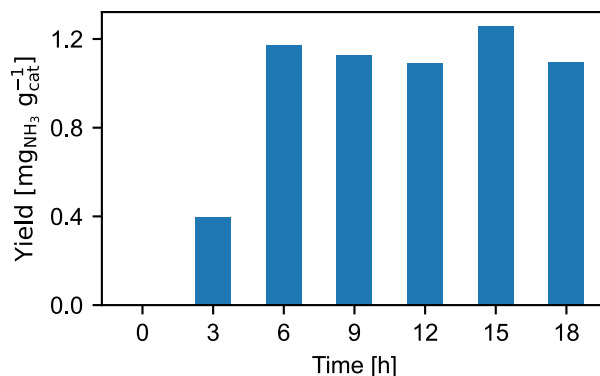
Figure 1: Ammonia concentration on the catalyst surface after milling times between 0 and 18 h, as measured by ion chromatography (IC).

Nitrogen physisorption verified that a rapid increase in catalyst surface area occurred in the first 6 h of milling, followed by only a slight increase during the 6 to 12 h period and possible particle agglomeration at milling times between 15 and 18 h (Figure 2a). Therefore, in addition to TiN catalyst formation, the initial increase in ammonia yield and subsequent stagnation can be attributed to the increase in surface area. The pore size distribution showed that the formation of pores with sizes below 50 nm contributed to the increased surface area (Figure 2b). These pores are attributed to the interstitial space between agglomerated nanoparticles. The greatest pore volume was observed after 12 h, before a small decrease in particle surface area occurred, which can be explained by the formation of a denser nitride phase. The correlation of ammonia yield and surface area was analyzed to determine the surface ammonia saturation. The ammonia uptake at 3 h was 0.027 mg m^{-2}, while from 6 h to 18 h, the ammonia surface coverage fluctuated around an average value of 0.036 mg m^{-2}. Thus, while the increased surface area explains a significant part of the increased ammonia uptake, there was also an increase in the surface area normalized ammonia uptake when the milling time was increased from 3 to 6 h. This is most likely due to gradual formation of new sites for ammonia formation and adsorption in the initial stages of milling.
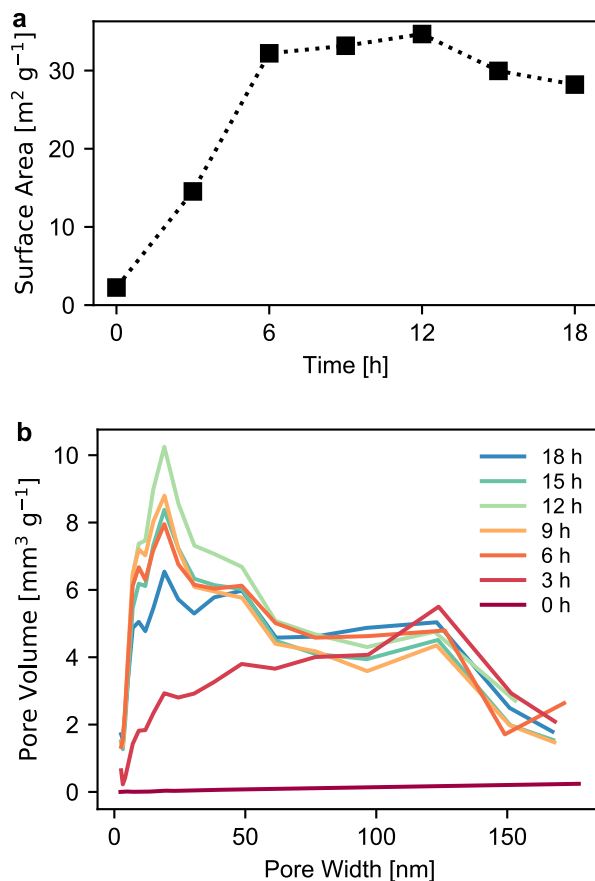
Figure 2: (a) Progression of BET surface area of during milling up to 18 h. (b) Development of pore volume distribution with milling time.

Initially, the pure Ti metal particles had a smooth, nonporous surface and particle sizes exceeding 100 μm (Figure 3a). Upon milling, the particle size decreased, which likely increased the amount of surface defects. The contrast between the samples after 0 and 3 h (Figure 3a-b) showed a distinct change in particle roughness and porosity. Additionally, SEM/EDS analysis of the samples was used to semi-quantitatively study the progression of nitrogen incorporation into the Ti (Figure 3c). A significant portion of the final nitrogen content is incorporated within the first 3 h of milling. Importantly, EDS analysis of pure TiN showed a N:Ti ratio of 31:69 (0.5), suggesting the milled Ti did reach full conversion to a nitride. After 3 h, larger solid particles appeared to be covered with smaller particles, while after 6 h, larger TiN particles were constituted of agglomerated nanoparticles (Figure 3d). This observation aligns well with the significant increase in pore volume after 6 h. TEM images showed that the TiN particles after 6 h of milling had an average diameter of 24 nm. The particles roughly retained this size during additional milling, as the particles after 12 h of milling had a diameter of 28 nm (Figure 3e). Thus, constant fracturing and sintering of TiN particles led to an equilibrium particle size distribution as commonly observed in grinding processes.[47, 48] However, after 18 h of milling, particles began to agglomerate and increased to 44 nm (Figure 3f). This is supported by the slight decrease in surface area and the collapse of pore volume between 12 h and 18 h. Additionally, small particles were observed in the TEM images of the sample after 18 h. Based on the Z-contrast, these are believed

to be iron particles from the milling vessel. Overall, with the complete nitridation and increase in surface area, the catalyst would be expected to reach its highest activity by 6 h and to sustain this activity for the next several hours. However, the agglomeration of particles and loss of pore volume may indicate that a catalyst might begin to lose activity at extended milling times.
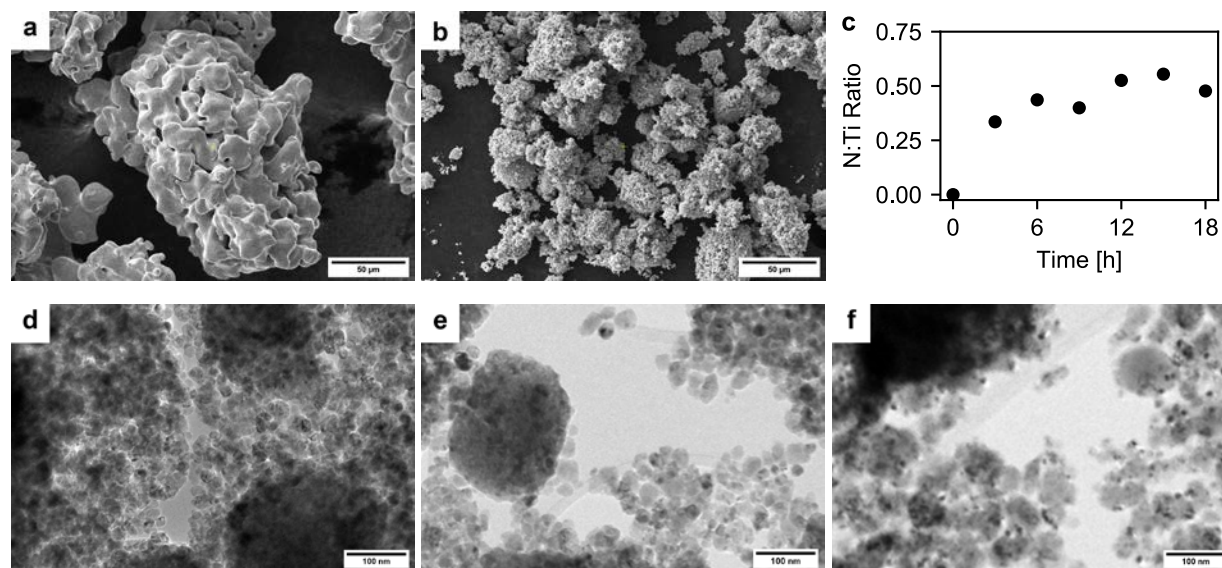

Figure 3: SEM images of (a) the starting Ti and (b) after milling for 3 h in N_2 and H_2. (c) Ratio of N to Ti over the course of milling, as measured by EDS. TEM images of TiN after milling for (d) 6 h, (e) 12 h, and (f) 18 h.

X-ray powder diffraction patterns were collected for the titanium metal pre-catalyst (0 h), the milled samples from 3 h to 18 h, and a TiN standard (Figure 4a-b). Titanium nitride can be readily distinguished from metallic titanium via the two peaks at 36.7° and 42.6°, corresponding to the (111) and (200) planes, respectively.[49, 50] In this region, metallic titanium has three peaks at 35.1°, 38.4°, and 40.1° resulting from the (100), (002), and (101) planes.[51] Within 3 h of milling, the XRD pattern was dominated by the titanium nitride peaks, and no characteristic peaks for titanium metal were observed. The peaks in the milled samples were broad and exhibited a low signal-to-noise ratio, suggesting the presence of very small crystallite domains and highly amorphous structures overall, especially in comparison to the unmilled titanium metal and commercial titanium nitride. These results align with the attrition of the large titanium particles observed via SEM and the formation of nanometer sized particles seen via TEM imaging. The changes in the peak positions and the average crystallite size over the course of milling can provide additional insights (Figure 4c-e). After 3 h, the lattice spacing in mechanochemically synthesized titanium nitride was more compressed compared to the titanium nitride standard, as shown by a shift in peak positions to larger diffraction angles. With increasing milling time, a general decrease of the d-spacing was observed, corresponding to further compression of the crystal lattice. This effect can potentially be attributed to a loss of lattice nitrogen, which has been shown to result in smaller lattice parameters in TiN.[52] The larger widths of the peaks also showed that the mechanochemically prepared samples were more amorphous than the TiN standard. The average

crystallite size nearly doubled from approximately 6 nm to 10 nm between 3 h and 6 h, after which the crystallite size remained stable. From this analysis and TEM imaging, it can be determined that the mechanochemically prepared TiN only has 2 to 3 crystal domains per particle.
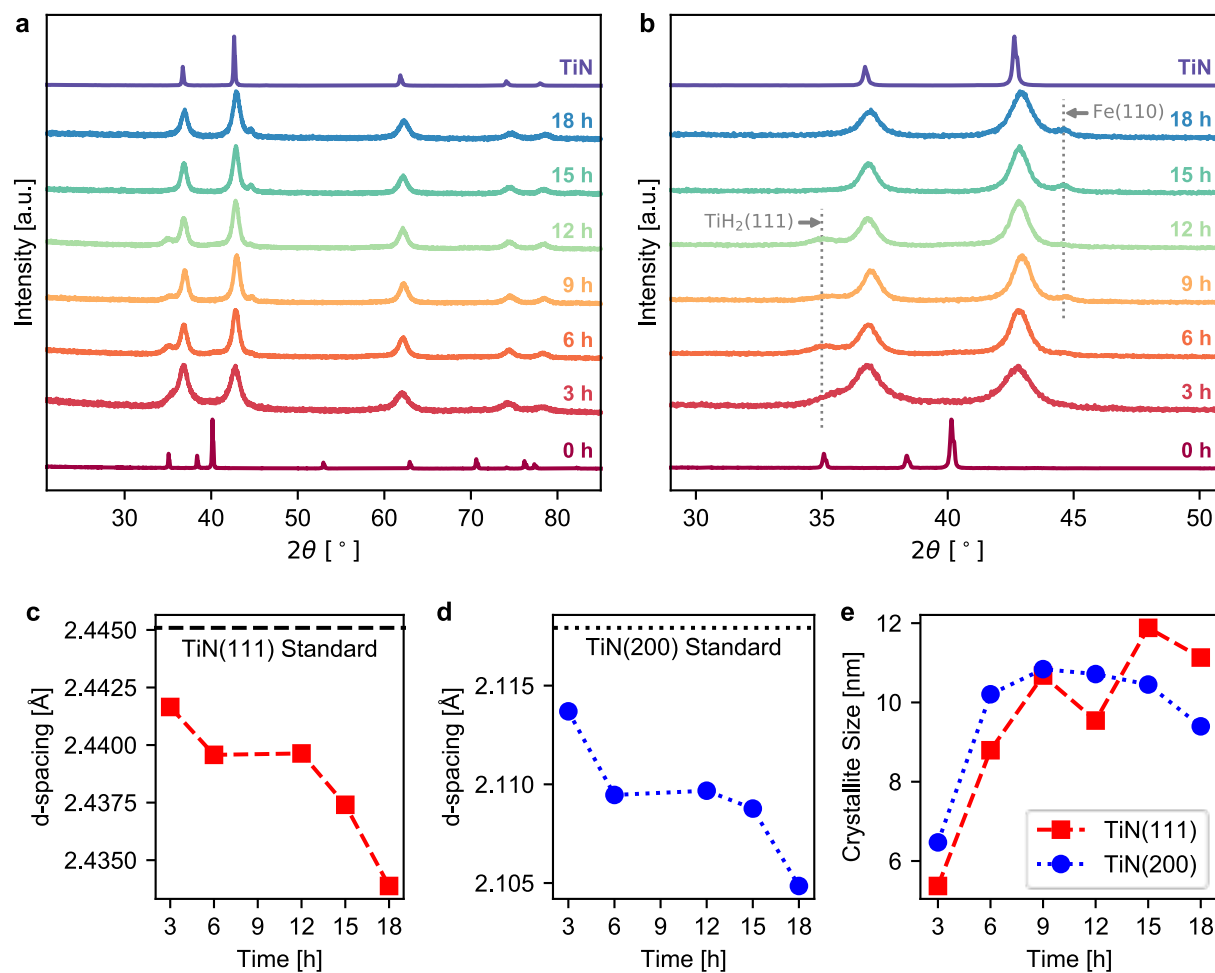

Figure 4. (a-b) X-ray diffractograms of the initial titanium metal, the progression of the titanium milled in N_2 and H_2 up to 18 h, and commercial titanium nitride. d-spacing for (c) the TiN(111) plane and (d) the TiN(200) plane over the course of milling and for the TiN standard (dashed line). (e) Average crystallite size calculated from the TiN(111) and TiN(200) peak widths over the course of milling.

A small shoulder was observed at 35.0° in the samples between 3 h and 12 h of milling (Figure 4b). While the peak positions correspond to Ti(110), the absence of the characteristic Ti(101) peak at 40.1° suggests another source. Instead, this peak is attributed to the (111) plane of titanium hydride (TiH$_2$),[53][50] which can form in the presence of H_2.[54] The intensity of the hydride peak diminished with milling as it was converted to the more stable nitride. For the samples after 9, 12, 15, and 18 h, a small peak was observed at 44.6°, which corresponds to the (110) plane of metallic iron.[55] Since the milling vessel and ball are a made of stainless steel, small amounts of shavings are expected to be generated and become physically mixed with the titanium nitride powder. These contaminations were also observed in TEM (Figure 3f).

Conclusion

In our previous work, we showed that the yield of adsorbed ammonia increases as function of milling time, following a gradual conversion of Ti to the TiN catalyst. This study illustrates the structural development of the TiN catalyst and its transient sites as a function of milling time. The largest changes in adsorbed ammonia occur between 3 and 6 h of milling, whereas the concentration of surface ammonia remains constant when the milling time is extended to 18 h, indicating that the surface structure of the catalyst has achieved a steady state. Net titanium nitride formation occurs during the first 6 h, while during extended milling any additional nitride formation is balanced by hydrogenation of nitrides to ammonia. Furthermore, physico-chemical characterization illustrates a large increase in surface area and pore volume in the first 6 h of milling as Ti/TiN is fractured into small particles of approximately 30 nm which, attached to each other, form porous agglomerates ranging from 0.1 to 5 μm. After this period, particle fracturing and sintering reached an equilibrium. A contraction of the TiN crystal lattice, as observed by XRD, suggested the loss of lattice nitrogen from TiN over the course of milling. Future work should focus on investigating meta-stable nitrides and the impact of process conditions to co-optimize the rates of nitride formation and conversion.

Author Contributions

J.A.D. performed the mechanochemical reactions and ammonia characterization. E.V.P. collected XRD, TEM and SEM data. J.A.D., E.V.P., K.L.H. and A.W.T. contributed to writing the original draft. C.S. and A.W.T. supervised the project and interpreted results. The manuscript was carefully revised by all authors.

Conflicts of Interest

There are no conflicts to declare.

Acknowledgements

References

1. K. H. Rouwenhorst, A. S. Travis and L. Lefferts, *Sustain. Chem.*, 2022, **3**, 149-171.
2. C. Smith, A. K. Hill and L. Torrente-Murciano, *Energy Environ. Sci.*, 2020, **13**, 331-344.
3. M. Appl, in *Ullmann's Encyclopedia of Industrial Chemistry*, WILEY-VCH Verlag GmbH & Co. KGaA, Weinheim, 2006.
4. N. Saadatjou, A. Jafari and S. Sahebdelfar, *Chem. Eng. Commun.*, 2015, **202**, 420-448.
5. J. Hargreaves, *Appl. Petrochem. Res.*, 2014, **4**, 3-10.

6. D. Mckay, J. Hargreaves, J. Rico, J. Rivera and X.-L. Sun, *J. Solid State Chem.*, 2008, **181**, 325-333.
7. A. Mittasch and W. Frankenburg, in *Adv. Catal.*, Elsevier, 1950, vol. 2, pp. 81-104.
8. N. Segal and F. Sebba, *J. Catal.*, 1967, **8**, 105-112.
9. D. King and F. Sebba, *J. Catal.*, 1965, **4**, 253-259.
10. R. Kojima and K.-i. Aika, *Appl. Catal. A-Gen.*, 2001, **209**, 317-325.
11. G. Panov and A. Kharitonov, *React. Kinet. Catal. Lett.*, 1985, **29**, 267-274.
12. S. Al Sobhi, N. Bion, J. S. J. Hargreaves, A. L. Hector, S. Laassiri, W. Levason, A. W. Lodge, A. R. McFarlane and C. Ritter, *Mater. Res. Bull.*, 2019, **118**, 5.
13. C. J. Jacobsen, S. Dahl, B. S. Clausen, S. Bahn, A. Logadottir and J. K. Nørskov, *J. Am. Chem. Soc.*, 2001, **123**, 8404-8405.
14. N. Bion, F. Can, J. Cook, J. Hargreaves, A. L. Hector, W. Levason, A. McFarlane, M. Richard and K. Sardar, *Appl. Catal. A: Gen.*, 2015, **504**, 44-50.
15. A. J. Medford and M. C. Hatzell, *ACS Catal.*, 2017, **7**, 2624-2643.
16. G. Duan, Y. Chen, Y. Tang, K. A. Gasem, P. Wan, D. Ding and M. Fan, *Prog. Energy Combust. Sci.*, 2020, **81**, 100860.
17. P. M. Barboun and J. C. Hicks, *Annu. Rev. Chem. Biomol. Eng.*, 2020, **11**.
18. M. C. Hatzell, *ACS Energy Lett.*, 2022, **7**, 4132-4133.
19. J. C. Whitehead, in *Plasma Catalysis*, Springer, 2019, pp. 343-348.
20. P. Balaz, M. Achimovicova, M. Balaz, P. Billik, Z. Cherkezova-Zheleva, J. M. Criado, F. Delogu, E. Dutkova, E. Gaffet, F. J. Gotor, R. Kumar, I. Mitov, T. Rojac, M. Senna, A. Streletskii and K. Wieczorek-Ciurowa, *Chem. Soc. Rev.*, 2013, **42**, 7571-7637.
21. V. Boldyrev and K. Tkáčová, *J. Mater. Synth. Process.*, 2000, **8**, 121-132.
22. T. Friščić, *J. Mater. Chem.*, 2010, **20**, 7599-7605.
23. G. W. Wang, *Chem Soc Rev*, 2013, **42**, 7668-7700.
24. D. E. Crawford, L. Wright, S. James and A. Abbott, *ChemComm*, 2016, **52**, 4215-4218.
25. L. Sharma, D. Kiani, K. Honer and J. Baltrusaitis, *ACS Sustain. Chem. Eng.*, 2019, **7**, 6802-6812.
26. C. Duan, L. Hu and J. Ma, *J. Mater. Chem. A*, 2018, **6**, 6309-6318.
27. V. Štrukil, *ChemSusChem*, 2021, **14**, 330-338.
28. A. W. Tricker, A. A. Osibo, Y. Chang, J. X. Kang, A. Ganesan, E. Anglou, F. Boukouvala, S. Nair, C. W. Jones and C. Sievers, *ACS Sustain. Chem. Eng.*, 2022, **10**, 11338-11347.
29. F. Schüth, R. Rinaldi, N. Meine, M. Käldström, J. Hilgert and M. K. Rechulski, *Catal. Today*, 2014, **234**, 24-30.
30. A. D. Brittain, N. J. Chrisandina, R. E. Cooper, M. Buchanan, J. R. Cort, M. V. Olarte and C. Sievers, *Catal. Today*, 2018, **302**, 180-189.
31. M. Yabushita, H. Kobayashi, K. Kuroki, S. Ito and A. Fukuoka, *ChemSusChem*, 2015, **8**, 3760-3763.
32. A. W. Tricker, G. Samaras, K. L. Hebisch, M. J. Realff and C. Sievers, *Chem. Eng. J.*, 2020, **382**, 122954.
33. S. Immohr, M. Felderhoff, C. Weidenthaler and F. Schüth, *Angew. Chem. Int. Ed. Engl.*, 2013, **52**, 12688-12691.
34. R. Eckert, M. Felderhoff and F. Schüth, *Angew. Chem. Int. Ed. Engl.*, 2017, **56**, 2445-2448.
35. M. Roldan, V. López-Flores, M. Alcala, A. Ortega and C. Real, *J. Eur. Ceram. Soc.*, 2010, **30**, 2099-2107.
36. N. J. Welham, T. Kerr and P. E. Willis, *J. Am. Ceram. Soc.*, 1999, **82**, 2332-2336.
37. C. J. Jacobsen, J. Zhu, H. Lindeløv and J. Jiang, *J. Mater. Chem.*, 2002, **12**, 3113-3116.
38. G. Heinicke, K. Meyer and U. Senzky, *Z. Anorg. Allg. Chem.*, 1961, **312**, 180-185.
39. P. A. Thießen, G. Heinicke and N. Bock, *Z. Chem.*, 1974, **14**, 76.
40. A. W. Tricker, K. L. Hebisch, M. Buchmann, Y.-H. Liu, M. Rose, E. Stavitski, A. J. Medford, M. C. Hatzell and C. Sievers, *ACS Energy Lett.*, 2020, **5**, 3362-3367.

41.	G.-F. Han, F. Li, Z.-W. Chen, C. Coppex, S.-J. Kim, H.-J. Noh, Z. Fu, Y. Lu, C. V. Singh and S. Siahrostami, *Nat. Nanotechnol.*, 2021, **16**, 325-330.
42.	S. Reichle, M. Felderhoff and F. Schüth, *Angew. Chem. Int. Ed.*, 2021, **60**, 26385-26389.
43.	C. He, Q. Li, X. Zhang, Y. Lu, D. Qiu, Y. Chen and X. Cui, *ACS Sustain. Chem. Eng.*, 2022, **10**, 746-755.
44.	Y. Sawama, M. Niikawa and H. Sajiki, *J. Synth. Org. Chem Jpn.*, 2019, **77**, 1070-1077.
45.	Y. Sawama, T. Kawajiri, M. Niikawa, R. Goto, Y. Yabe, T. Takahashi, T. Marumoto, M. Itoh, Y. Kimura and Y. Monguchi, *ChemSusChem*, 2015, **8**, 3773-3776.
46.	S. Brunauer, P. H. Emmett and E. Teller, *J. Am. Chem. Soc.*, 1938, **60**, 309-319.
47.	A. Bor, B. Jargalsaikhan, K. Uranchimeg, J. Lee and H. Choi, *Powder Technol.*, 2021, **394**, 181-190.
48.	H. Yu, Y. Sun, L. Hu, H. Zhou and Z. Wan, *Mater. Des.*, 2016, **104**, 265-275.
49.	Data retrieved from the Materials Project for TiN (mp-492) from database version v2021.11.10., https://materialsproject.org/materials/mp-492?chemsys=Ti-N#diffraction_patterns, November 2022), DOI: 10.17188/1208488.
50.	A. Jain, S. P. Ong, G. Hautier, W. Chen, W. D. Richards, S. Dacek, S. Cholia, D. Gunter, D. Skinner and G. Ceder, *APL Mater.*, 2013, **1**, 011002.
51.	Data retrieved from the Materials Project for Ti (mp-46) from database version v2021.11.10., https://materialsproject.org/materials/mp-46?formula=Ti#diffraction_patterns, November 2022), DOI: 10.17188/1208281.
52.	M. Lebeda, P. Vlčák and J. Drahokoupil, *Comput. Mater. Sci.*, 2022, **211**, 111509.
53.	Data retrieved from the Materials Project for TiH_2 (mp-24161) from database version v2021.11.10., https://materialsproject.org/materials/mp-24161?chemsys=Ti-H#diffraction_patterns, November 2022), DOI: 10.17188/1199952.
54.	J. Huot, D. B. Ravnsbæk, J. Zhang, F. Cuevas, M. Latroche and T. R. Jensen, *Prog. Mater Sci.*, 2013, **58**, 30-75.
55.	Data retrieved from the Materials Project for Fe (mp-13) from database version v2021.11.10., https://materialsproject.org/materials/mp-13?chemsys=Fe#diffraction_patterns, November 2022), DOI: 10.17188/1189317.